INTERNATIONAL JOURNAL FOR NUMERICAL METHODS IN FLUIDS, VOL. 18, 415–432 (1994)

SOLUTION OF THE AXISYMMETRIC INVERSE PROBLEM BY HIGHER-ORDER LINE DOUBLETS

M. F. ZEDAN

Mechanical Engineering Department, King Saud University, PO Box 800, Riyadh 11421, Saudi Arabia

SUMMARY

The axial singularity inverse method for designing bodies of revolution has been improved by using higher-order doublet elements. The performance of the method for various element orders and other solution parameters is presented in detail. The results indicate that the method is generally more robust, less sensitive to insets and has a better-conditioned coefficient matrix compared with the source method of the same order. The condition number of the matrix is shown to increase with the thickness of the body, the order of the method, the number of elements and the degree of stretching of the node distribution. In general, good performance is attained for most bodies even with f_r as low as 2 by using 10–12 second-order doublet elements with insets greater than $0{\cdot}02L$ from rounded ends. Increasing the insets to $0{\cdot}06L$ appears to improve the accuracy of the method for most bodies but slows its convergence.

KEY WORDS Aerodynamics Aerodynamic design Inverse problems Body shaping

1. INTRODUCTION

In the direct approach of aerodynamic design a component shape is manipulated either manually based on experience or by using an optimization scheme to achieve design goals. In the inverse approach the pressure (or velocity) distribution is manipulated and the corresponding body geometry is obtained. The inverse approach is much more effective than the direct one, since the aerodynamic characteristics of a body are easier to relate to its pressure distribution than to its shape. Inverse design techniques have been successfully used for some time in designing 2D aerodynamic shapes such as high-lift[1] and low-drag aerofoils.[2] The use of these techniques for bodies of revolution has been fairly limited so far because of two reasons. First, these bodies are not intended to generate lift, leaving drag reduction as the primary design objective. The potential for drag reduction by delaying transition has been very small owing to surface finish limitations and high Reynolds number. With new manufacturing techniques and materials the surface finish limitation is not valid any more for a growing number of applications such as small aircraft fuselages,[3] external stores and torpedoes. The second reason is the lack of an efficient and robust solution for the axisymmetric inverse problem. The available solutions are necessarily iterative because of the unknown boundary. Surface singularities are used to represent the body in one class of methods,[4,5] while line sources distributed along the body axis are used in another.[6] Surface singularity methods appear to be more robust and can handle a wider range of shapes, while the axial source method is computationally much more efficient. This latter method typically converges in four iterations compared with 10–24 iterations for surface singularity methods, with much fewer computations per iteration. However, the method often produces ill-conditioned matrices and is sensitive to the number and distribution of elements

CCC 0271–2091/94/040433–18

Received December 1992
Revised October 1993

and control points for thick bodies and for bodies with sudden changes in curvature. Sensitivity to the distance between the ends of the singularity distribution and body ends (insets) has also been reported.

The objective of this paper is to make the axial singularity method more robust over a wide range of geometries while retaining its simplicity and computational efficiency. This is achieved by exploring the use of high-order line doublet elements to represent the body instead of the currently used line source elements. The use of doublets to represent bodies of revolution is not new; however, it has been limited to the solution of the direct problem. Only recently the author and his colleagues[7] used linear doublet elements in an inverse method to design low-drag fuselage shapes. However, the performance of that method was not studied. In the present work the inverse method is extended to utilize doublet elements with an arbitrary (polynomial) intensity distribution. The performance of the method is then investigated for various orders of distribution and other solution parameters and is compared with that of the source method using carefully chosen test cases.

2. RELATED STUDIES

The surface source method of Bristow[4] appears to be the first inverse method for bodies of revolution (1974). In that method the body geometry is updated in each iteration such that the mean square difference between the prescribed velocity distribution and the velocity distribution calculated by the Douglas–Neumann surface source method is reduced. The method converged nicely in 10 iterations in the three examples presented by Bristow.[4] Another surface singularity inverse method has been presented very recently (1991) by Dinavahi and Chow.[5] The method employs surface vortex sheets and has an iterative scheme very similar to that of Zedan and Dalton,[6] thus eliminating the need to solve the direct problem in every iteration as in Bristow's method. While this reduced the calculations per iteration, the method needed 24 iterations to converge in most of the test cases presented, even after using a weighting factor to accelerate convergence.

Three years after Bristow's method, Zedan and Dalton[6] presented a much simpler solution in which the body is represented by line source elements along its axis, each with constant intensity. The method converged nicely in four iterations for simple body shapes. Elements with linearly varying strength[8] were used later to extend the range of application of the method to bodies with an inflection point. Higher-order source elements[9] were also investigated for both direct and inverse problems. The study showed that the performance of the method for a particular element order improves as the number of elements increases up to an optimum number beyond which the solution deteriorates. Since that work[9] was published in 1980, a number of studies on optimizing the axial singularity distribution for solving the direct problem have appeared but none for the inverse problem. These efforts include optimization of the location of point sources along the axis,[10] use of least squares procedures[11] and other smoothing techniques[12] to determine the singularity distribution and a study[13] on the effect of insets, the number and distribution of elements as well as the use of doublet elements instead of source elements for axial flow. Recently[14] it has been shown that the use of linear doublet elements provides a more robust and generally more accurate solution to the direct problem. This study also showed that the matrix of doublet direct methods has a condition number an order of magnitude smaller than that for source methods, thus allowing the use of a higher number of elements. This provides a better representation of bodies over a wider range of geometry and fineness ratio.

The above efforts are generally lacking for the inverse method. The only exception is the

recent use of linear doublet elements to solve the inverse problem.[7] However, this inverse doublet method was only derived for elements with linear (or constant) distribution. Based on limited test cases, the method was shown to be promising; however, its performance was neither evaluated for various solution parameters nor for 'difficult' body shapes.

3. MATHEMATICAL DESCRIPTION

Axial flow around an axisymmetric body may be obtained by adding a uniform stream with velocity V_∞ to a distribution of line doublets of intensity μ_x between x_n and x_t along the body axis. The doublet distribution is discretized into elements as shown in Figure 1. In the element co-ordinate system the streamfunction of an element is

$$\psi = \int_0^l \frac{-\eta^2 \mu_\zeta \, d\zeta}{[(\xi - \zeta)^2 + \eta^2]^{3/2}}, \tag{1}$$

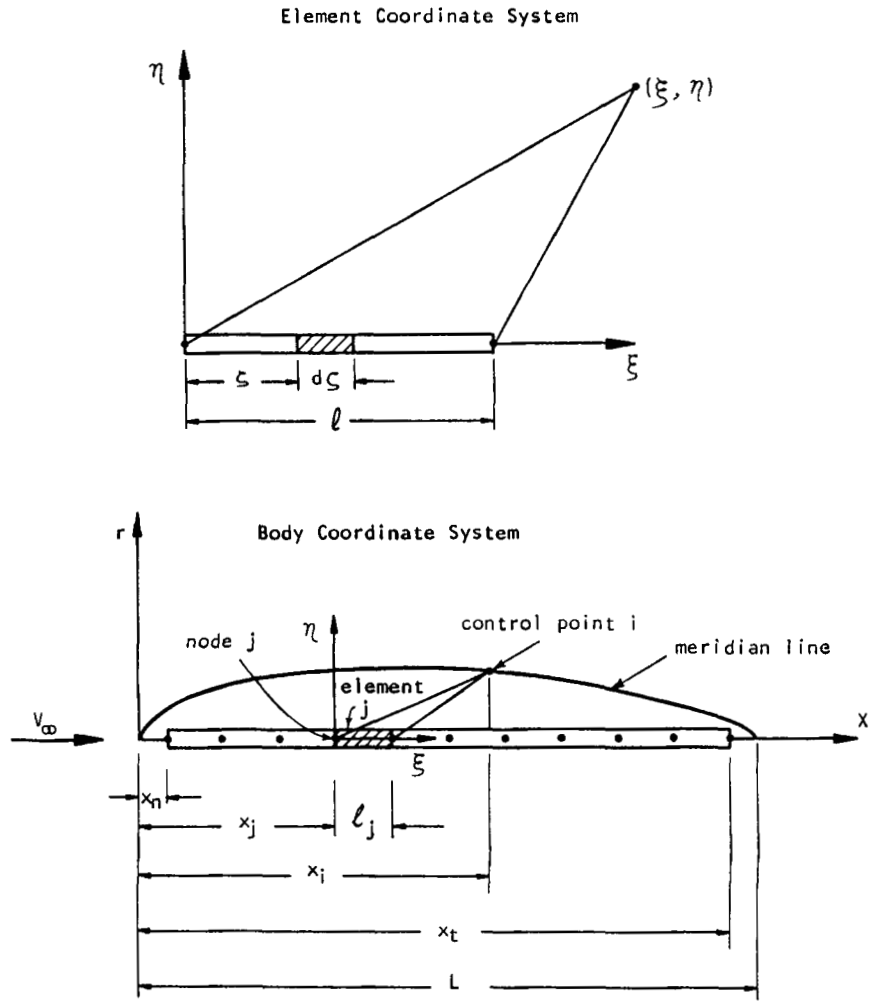

Figure 1. Definition sketch of elements, control points and co-ordinate systems

where μ_ζ is the element doublet intensity distribution. The velocity components induced by this element are obtained by differentiating ψ. The resulting expressions are

$$u = 3\eta^2 \int_0^l \frac{\mu_\zeta \, d\zeta}{[(\zeta - \zeta)^2 + \eta^2]^{5/2}} - 2 \int_0^l \frac{\mu_\zeta \, d\zeta}{[(\xi - \zeta)^2 + \eta^2]^{3/2}}, \tag{2}$$

$$v = -3\eta \int_0^l \frac{\mu_\zeta(\xi - \zeta) \, d\zeta}{[(\xi - \zeta)^2 + \eta^2]^{5/2}}. \tag{3}$$

The intensity distribution over the element is represented by a polynomial of degree v,

$$\mu_\zeta = \sum_{k=1}^{v+1} a_k \zeta^{k-1} \tag{4}$$

Substituting μ_ζ from equation (4) into equations (2)–(3), one obtains

$$\psi(\xi, \eta) = -\eta^2 \sum_{k=1}^{v+1} a_k H_{k-1}, \tag{5a}$$

$$u(\xi, \eta) = 3\eta^2 \sum_{k=1}^{v+1} a_k P_{k-1} - 2 \sum_{k=1}^{v+1} a_k H_{k-1}, \tag{5b}$$

$$v(\xi, \eta) = 3\eta \sum_{k=1}^{v+1} a_k (P_k - \xi P_{k-1}), \tag{5c}$$

where

$$H_k(\xi, \eta) = \int_0^l \frac{\zeta^k \, d\zeta}{[(\xi - \zeta)^2 + \eta^2]^{3/2}}, \tag{6a}$$

$$P_k(\xi, \eta) = \int_0^l \frac{\zeta^k \, d\zeta}{[(\xi - \zeta)^2 + \eta^2]^{5/2}}. \tag{6b}$$

Fortunately, these integrals can be evaluated in closed form as given in Appendix II. The flow field around the axisymmetric body at a point (x, r) is obtained by adding the uniform flow to the contributions of all elements. At a control point i on the body surface we have

$$\psi_i = V_\infty \frac{r_i^2}{2} + \sum_{j=1}^{n_e} \left(-\eta_i^2 \sum_{k=1}^{v_j+1} a_{jk} H_{k-1}(\xi_i, \eta_i) \right), \tag{7a}$$

$$u_i = V_\infty + \sum_{j=1}^{n_e} \left(\sum_{k=1}^{v_j+1} a_{jk} [3\eta^2 P_{k-1}(\xi_i, \eta_i) - 2H_{k-1}(\xi_i, \eta_i)] \right), \tag{7b}$$

$$v_i = 3r_i \sum_{j=1}^{n_e} \left(\sum_{k=1}^{v_j+1} a_{jk} [P_k(\xi_i, \eta_i) - \xi_i P_{k-1}(\xi_i, \eta_i)] \right), \tag{7c}$$

where

$$\xi_i = x_i - x_j, \qquad \eta_i = r_i, \tag{8}$$

x_j is the x-coordinate of the leading edge of element j in the body co-ordinate system, v_j is the

degree of the polynomial distribution of element j and a_{jk} with $k = 1$ to v_j represent the unknown coefficients of the polynomial distribution of element j. Equations (7) are recast in the form

$$\psi_i = V_\infty \frac{r_i^2}{2} + \sum_{m=1}^{N} \bar{\psi}_{im} c_m, \tag{9a}$$

$$u_i = V_\infty + \sum_{m=1}^{N} \bar{U}_{im} c_m, \tag{9b}$$

$$v_i = \sum_{m=1}^{N} \bar{V}_{im} c_m, \tag{9c}$$

where

$$N = n_e + \sum_{j=1}^{n_e} v_j \tag{10}$$

and c_m represent the unknown polynomial coefficients a_{jk} of all elements after being arranged in one array. Note that the influence matrices $\bar{\psi}$, $\bar{U}$ and $\bar{V}$ are functions of the geometry only. The continuity of the distribution at the node between elements j and $j + 1$ requires

$$\sum_{k=1}^{v_j+1} a_{jk} l_j^{k-1} = a_{j+1,1}. \tag{11}$$

We have $n_e - 1$ such conditions for $j = 1$ to $n_e - 1$.

The solution of the inverse problem from this point on follows essentially the iterative procedure given by Zedan and Dalton.[9] In brief, the procedure starts with an initial smooth geometry such as an ellipsoid of high fineness ratio for which the slopes $(dr/dx)_i$ at the control points and the matrices $\bar{\psi}_{ij}$, $\bar{U}_{ij}$ and $\bar{V}_{ij}$ are computed. The axial velocity components u_i at the control points on the body surface are obtained from the given velocity distribution by applying the tangency condition. The coefficients of the doublet distribution c_m for methods with order higher than zero are obtained by solving a system of linear equations consisting of equation (9b) applied at the control points in addition to the continuity condition (equation (11)) applied at the $n_e - 1$ nodes between elements. The best results for the present doublet method are obtained with $n_e + 1$ control points at the x-co-ordinates of the nodes and $v_j - 1$ control points evenly distributed over each element. In the zeroth-order method the continuity condition is not enforced and one control point per element at its middle is used. A new set of control point ordinates r_i is obtained by setting $\psi_i = 0$ on the body surface in equation (9a). This gives

$$r_i = \sqrt{\left(-\frac{2}{V_\infty} \sum_{m=1}^{N} \bar{\psi}_{im} c_m \right)}. \tag{12}$$

The computed values of r_i replace the previous geometry and the above procedure is repeated until convergence is attained. Note that convergence is determined based on the computed radius; for more discussion on convergence criteria the reader is referred to Reference 6.

4. RESULTS AND DISCUSSION

The doublet method described above and the source method[9] have been programmed on a PC-AT microcomputer. In both methods body co-ordinates are normalized by L, velocities by V_∞ and ψ by $V_\infty L^2$. The two programmes are identical with the exception of the subroutines forming the influence matrices and those setting up the control points. The control points are selected for the doublet method as described above. As for the source method,[9] v_j control points are uniformly distributed along each element; the system of equations to determine c_m is closed by satisfying the continuity condition at the $n_e - 1$ nodes between elements and by using the zero-net-source-efflux condition. These slightly different control point schemes for the doublet and source methods are chosen in order to give the best performance for each method. In the following presentation the doublet method is first calibrated and verified via test cases, then its performance is compared with that of the source method for various solution parameters.

4.1. Test cases

The first test case is the dumb-bell profile used recently by Hemsch[12] to verify direct problem solutions. The meridian line of this profile is described by

$$r/L = 2\varepsilon\sqrt{\{bX(1-X)[1-bX(1-X)]\}},$$

where $\varepsilon = r_{max}/L$ and b is a geometrical parameter. We chose a profile with $\varepsilon = 0{\cdot}11$ ($f_r = 4{\cdot}55$) and $b = 3$ (Figure 2(a)). Hemsch found this particular profile to be troublesome to the axial singularity direct method and therefore we think it is a challenge for the inverse method. A highly accurate velocity distribution for this body obtained by the author[14] was input to the

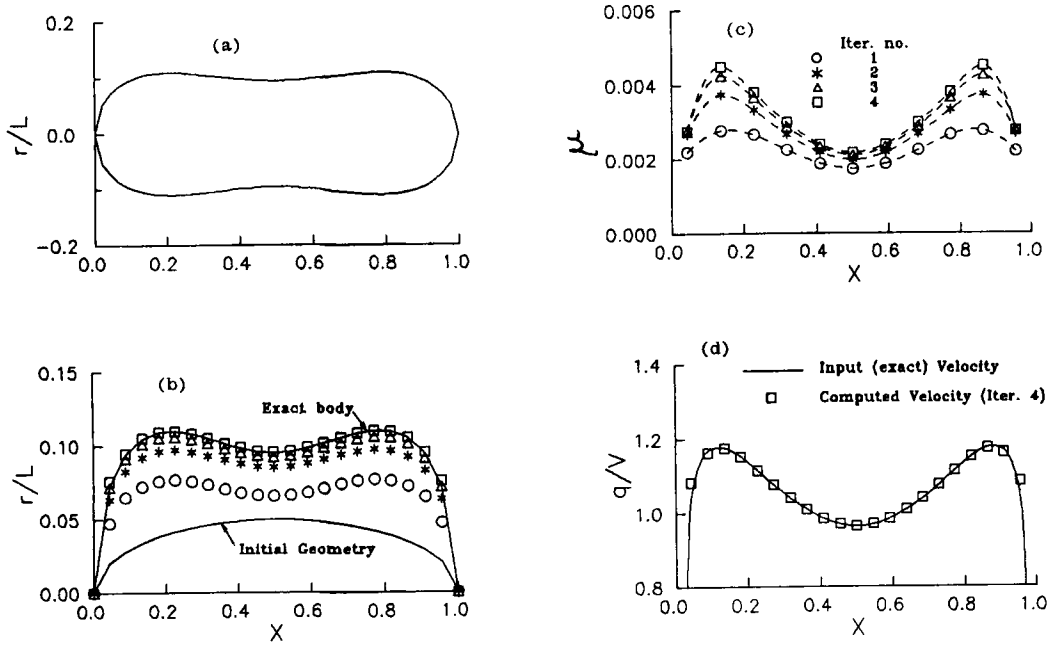

Figure 2. Second-order doublet solution for dumb-bell profile: (a) body shape; (b) meridian line; (c) doublet intensity distribution; (d) velocity distribution

doublet inverse method. Using 10 elements with a parabolic intensity distribution extending from $X_n = 0{\cdot}0433$ to $X_t = 0{\cdot}9567$, the computed radius converged to the exact profile in four iterations as shown in Figure 2(b). These values of X_n and X_t were obtained from expressions[12] derived for a source distribution on the basis of the slender body theory. The doublet distribution computed in various iterations is shown in Figure 2(c). Figure 2(d) shows almost perfect agreement between the input velocity and the velocity computed from the doublet distribution in iteration 4.

The second test case is a drop-shaped body which is thicker ($f_r = 2{\cdot}0$) than the dumb-bell profile. This body is formed by adding a point source and a line sink to a uniform stream[15] and therefore its velocity distribution can be calculated exactly. With X_n and X_t chosen as 0·04 and 0·98 respectively and using 10 parabolic elements, the inverse doublet method was used to compute this body. Figure 3(a) shows that the solution converged to the exact body in the fourth iteration, at which the computed velocity distribution agrees very well with the input (exact) velocity as shown in Figure 3(b).

4.2. *Performance of the method*

The results of the above test cases showed clearly that the doublet method works well for bodies with non-simple geometries as well as for thick bodies. However, the effect of input

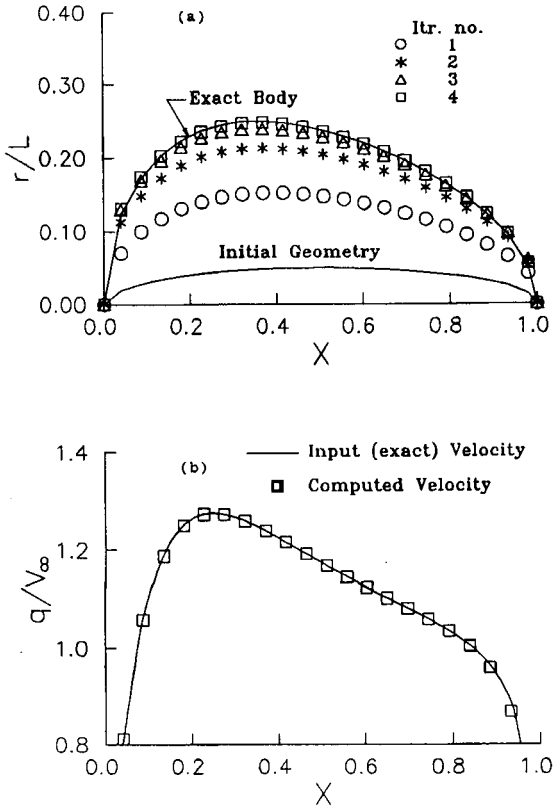

Figure 3. Second-order doublet solution for drop-shaped profile ($f_r = 2$): (a) convergence of computed radius; (b) comparison of input and computed velocity distributions

parameters such as X_n and X_t, the number and distribution of elements and the order of element distribution on the performance of the method is not known and is therefore studied below. Comparison is made with the performance of the source method[9] for which the effects of such parameters are also largely unknown, at least quantitatively. The performance is measured mainly in terms of the accuracy of the computed meridian line (radius). The speed of convergence and the condition number of the coefficient matrix are also of interest. Axial singularity methods are known to occasionally produce ill-conditioned matrices with adverse effects on accuracy. A condition number estimate (COND) is obtained by using the method of Reference 16. The matrix is considered 'computationally singular' for a particular computer if COND is so large that COND = COND + 1·0 on that machine. This corresponds to COND $\approx 10^8$ for the present machine. Lower values of COND indicate better-conditioned matrices. Although the doubtlet and source methods as derived allow the mixing of elements of various orders, we limit the discussion here to elements of the same order.

4.2.1. Effect of order of element intensity distribution. We investigate systematically doublet methods with orders zero to three and compare their performance with corresponding source methods[9] for a number of shapes. Only equal-length elements are used. The number of elements is chosen such that the number of algebraic equations remains the same for all orders. With 10 elements for the second-order method this gives 15 and 30 elements for the first- and zeroth-order methods respectively and approximately seven elements for the third-order method.

The first body is the dumb-bell profile discussed earlier. X_n and X_t are fixed at the 'correct' values (0·0433 and 0·9567) for this profile.[12] To condense the results, we present the root mean square of the error in the computed radius (r/L) at various iterations in Figure 4. The results for the iteration with minimum error are summarized in the left half of Table I. These results indicate that the accuracy of the doublet method improves as the order increases to the third. The third-order method gave an extremely low RMS error of $0{\cdot}487 \times 10^{-3}$. The performance of the source method does not show a consistent trend and is generally inferior to the doublet method except for the zeroth order. Also, for a given order the rate of convergence of the doublet method is equal to or faster than that of the source method. The condition number estimate (COND) of the coefficient matrix is shown in Figure 4(c). In general, doublet methods have lower COND than source methods of the same order. Also, the higher the order is, the larger COND is, with the exception of the linear source method which has lower COND than the zero-order source method. Figure 5(a) shows the doublet intensity distribution as computed at the nodes in the convergence iteration for various orders. The second- and third-order methods provide the smoothest variation, followed by the first-order method. The zeroth-order solution shows considerable oscillations near body ends. The corresponding results for the source methods in Figure 5(b) indicate a relatively smooth second-order solution, a first-order solution with some oscillations and highly oscillatory zeroth- and third-order solutions.

A similar investigation was made using the thick drop-shaped profile discussed earlier ($f_r = 2$). The RMS error in the computed radius at various iterations is shown in Figure 6(a). The minima of these RMS errors and corresponding iteration numbers are summarized in the left half of Table II. These results indicate that doublet methods are more accurate than source methods for all orders, with the third- and second-order methods being the most accurate, followed by the first- and zeroth-order methods respectively. As for the source methods, the third-order solution diverged because of a near-singular coefficient matrix, while the second- and first-order solutions have comparable accuracy. The condition number results presented in Figure 6(b) indicate that the third-order methods have the highest COND, followed by the second-order methods, while the first-order methods have the lowest values. We also observe that the values

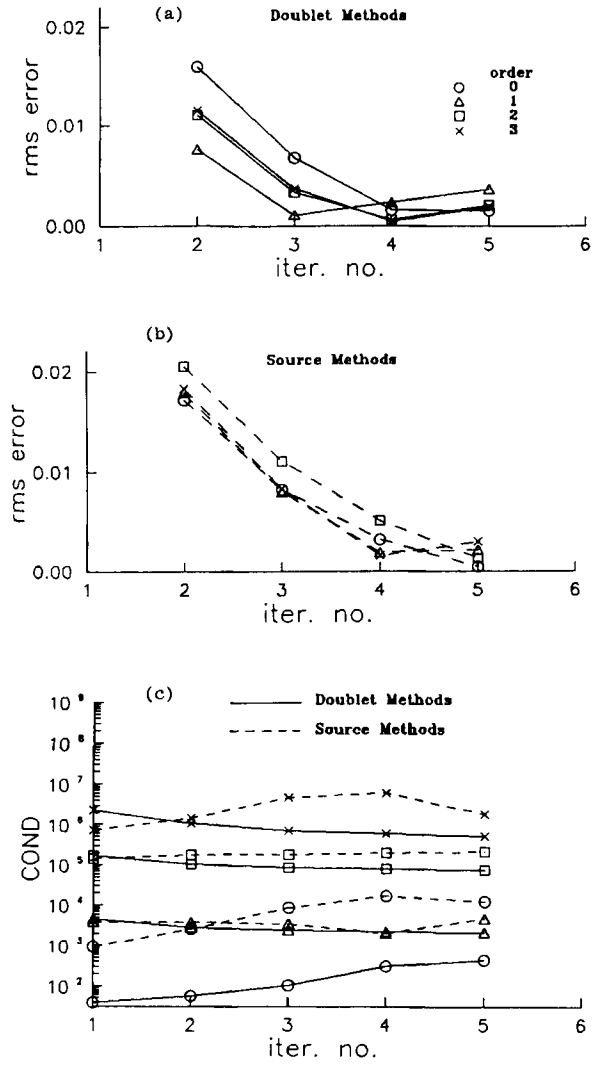

Figure 4. RMS error in radius of dumb-bell profile as computed by doublet and source methods of various orders at various iterations and corresponding condition number estimates

Table I: Effect of element order of distribution on the RMS error in computed radius and speed of convergence for the dumb-bell profile ($f_r = 4{\cdot}55$)

Element order	RMS error for $n_{eq} = 30$ (iter. no.)		RMS error for $n_c = 21$ (iter. no.)	
	Doublet	Source	Doublet	Source
3	$0{\cdot}487 \times 10^{-3}(4)$	$0{\cdot}1586 \times 10^{-2}(4)$	$0{\cdot}487 \times 10^{-3}(4)$	$0{\cdot}1586 \times 10^{-2}(4)$
2	$0{\cdot}6057 \times 10^{-3}(4)$	$0{\cdot}13007 \times 10^{-2}(5)$	$0{\cdot}6057 \times 10^{-3}(4)$	$0{\cdot}13007 \times 10^{-2}(5)$
1	$0{\cdot}112 \times 10^{-2}(3)$	$0{\cdot}1911 \times 10^{-2}(4)$	$0{\cdot}681 \times 10^{-3}(4)$	$0{\cdot}1309 \times 10^{-2}(5)$
0	$0{\cdot}152 \times 10^{-2}(5)$	$0{\cdot}424 \times 10^{-3}(5)$	$0{\cdot}410 \times 10^{-3}(4)$	$0{\cdot}1131 \times 10^{-2}(5)$

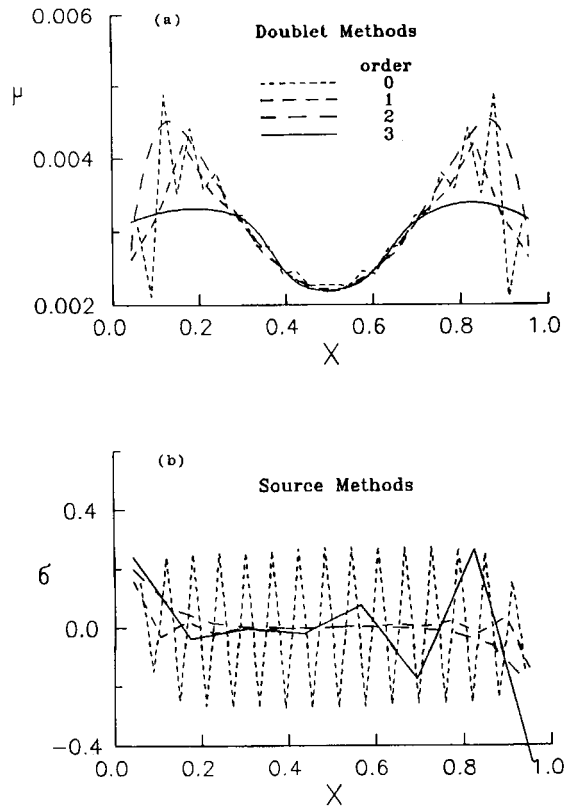

Figure 5. Computed singularity intensities at nodes in convergence iteration for case of Figure 4: (a) doublet methods; (b) source methods

of COND in Figure 6(b) are much higher than the corresponding values in Figure 4(c) for the dumb-bell profile. Moreover, the values of COND for doublet and source methods of the same order are much closer to each other in the present case. The reason for this may be the low fineness ratio of the drop-shaped profile used ($f_r = 2$).

The whole investigation was repeated for this body and for the dumb-bell profile while fixing the number of control points, n_c at nearly 21 for all orders (instead of fixing n_{eq} earlier). This corresponds to $n_e = 7$, 10, 20 and 20 elements for the third-, second-, first- and zeroth-order methods respectively. The RMS errors for the convergence (minimum error) iteration are shown in the right halves of Tables I and II. These results support the earlier conclusion that doublet methods are superior to source methods, especially for the thicker body. We also observe that the accuracy of the doublet methods generally improves as the order gets higher. However, we recommend that orders higher than the second should be avoided, because COND can assume dangerously high values, especially for thick bodies. The accuracy of the source methods improves as the order gets lower for the dumb-bell profile, while the first- and second-order solutions are the most accurate for the drop-shaped profile.

4.2.2. Effect of insets. The sensitivity of the solution to the choice of insets is more critical in the inverse problem than in the direct problem, since they are related to the derivatives of the

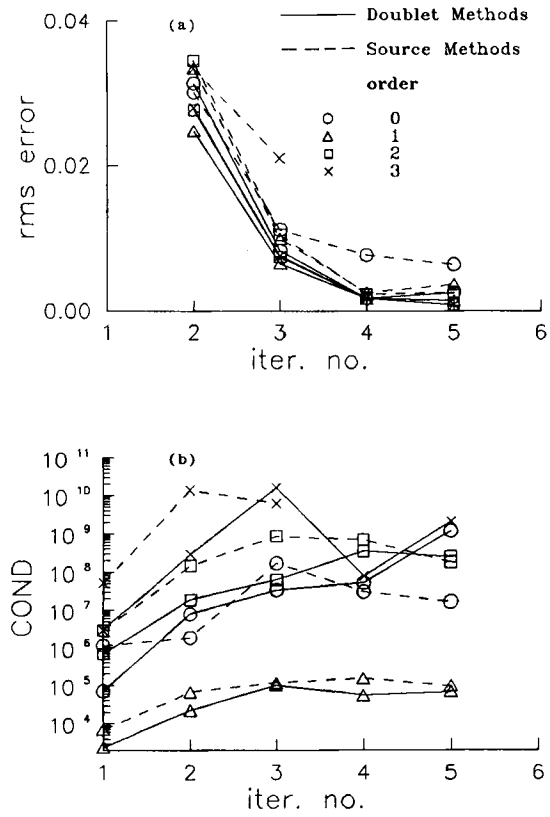

Figure 6. Inverse problem solution for drop-shaped profile ($f_r = 2$) by doublet and source methods of various orders: (a) RMS Error in computed radius; (b) condition number estimate of coefficient matrix

Table II. Effect of element order of distribution on the RMS error in computed radius and speed of convergence for the drop-shaped profile ($f_r = 2$)

	RMS error for $n_{eq} = 30$ (iter. no.)		RMS error for $n_c = 21$ (iter. no.)	
Element order	Doublet	Source	Doublet	Source
3	$0{\cdot}7873 \times 10^{-3}(6)$	Solution diverged	$0{\cdot}787 \times 10^{-3}(6)$	Solution diverged
2	$0{\cdot}8474 \times 10^{-3}(5)$	$0{\cdot}2330 \times 10^{-2}(4)$	$0{\cdot}847 \times 10^{-3}(5)$	$0{\cdot}233 \times 10^{-2}(4)$
1	$0{\cdot}1471 \times 10^{-2}(5)$	$0{\cdot}2553 \times 10^{-2}(4)$	$0{\cdot}855 \times 10^{-3}(5)$	$0{\cdot}245 \times 10^{-2}(4)$
0	$0{\cdot}176 \times 10^{-2}(4)$	$0{\cdot}642 \times 10^{-2}(5)$	$0{\cdot}181 \times 10^{-2}(4)$	Solution diverged

meridian line,[12] which is not known in advance in the inverse problem. Zedan and Dalton[6,8,9] used $X_n = 0{\cdot}02$ and $X_t = 0{\cdot}98$ in most of their studies without proper justification. Here we investigate the sensitivity of second-order inverse methods while fixing n_c at 10. The first test case is the dumb-bell profile used earlier. X_n and X_t are varied around the values obtained from the slender body expressions[12] ($X_n = 0{\cdot}0433$ and $X_t = 0{\cdot}9567$). Figure 7(a) shows the variation in the error in the computed radius at convergence along the body for $X_n = 0{\cdot}02$, $0{\cdot}0433$, $0{\cdot}06$

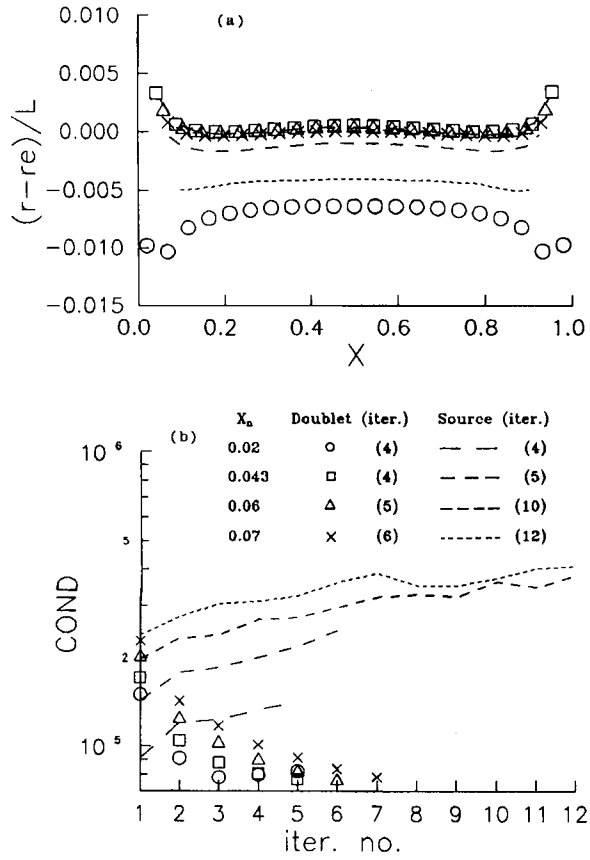

Figure 7. Effect of inset distance X_n on second-order doublet and source inverse solutions for dumb-bell profile: (a) error in computed radius; (b) matrix condition number estimate

and 0·07 and $X_t = 1 - X_n$. The doublet method is generally more accurate, less sensitive to X_n and converges faster than the source method for $X_n \geqslant 0{\cdot}0433$. In fact, the results of the doublet method are essentially unchanged for $X_n \geqslant 0{\cdot}0433$. The source method has its smallest error with $X_n = 0{\cdot}02$. The effect of X_n on the condition number of the matrix is smaller for the doublet method (Figure 7(b)), confirming the relative insensitivity of the method to this parameter compared with the source method, especially near convergence. We also notice that the greater X_n is, the higher the condition number is. This is because the control points become closer, thus decreasing the independence of the equations. The results in the figure confirm our earlier conclusion that the matrix of the doublet methods is better conditioned than that of the source methods. Also, it is observed that increasing the insets delays convergence somewhat for the doublet method and appreciably for the source method.

The effect of insets was also investigated for two ellipsoids (exact velocity distribution is known) with $f_r = 5$ and 2. The results (not presented) confirm that the doublet method is generally more accurate and less sensitive to X_n. On the other hand, the source solution for $f_r = 2$ deteriorated for $X_n > 0{\cdot}04$ and started diverging after iteration 5, in which it began losing its symmetry because of a near-singular coefficient matrix.

4.2.3. Effect of element distribution. This investigation is again limited to second-order methods. The dumb-bell profile is used as the test case with 10 elements extending from $X_n = 0{\cdot}0433$ to $X_t = 0{\cdot}9567$. The nodes between elements are located according to the exponential stretching of Hemsch,[12]

$$X_j = X_n + (1 - \rho^{j-1})(0{\cdot}5 - X_n)/(1 - \rho^{n_e/2}),$$

in the front half of the body with $j = 1, \ldots, n_e/2 + 1$ and $\rho = X_{j+1}/X_j$. The distribution in the rear half is similar. The amount of stretching depends on ρ; as ρ approaches unity, the nodes become equally spaced.

Figure 8(a) shows the variation in the error in the computed radius at convergence along the body for various schemes of node distribution. The results of the doublet method are spread around the zero error and closer to it than those of the source method, with the least errors obtained with $\rho = 1{\cdot}0$, followed by those with $\rho = 1{\cdot}1$ and $1{\cdot}2$ respectively. The smallest errors for the source method are obtained with $\rho = 1{\cdot}2$, but their distribution is not symmetric around $X = 0{\cdot}5$. The worst results for both methods are obtained with a cosine node distribution, which may be attributed to a two-order-of-magnitude jump in the matrix condition number (Figure 8(b)). In fact, it caused the source method to diverge after the second iteration. The error results

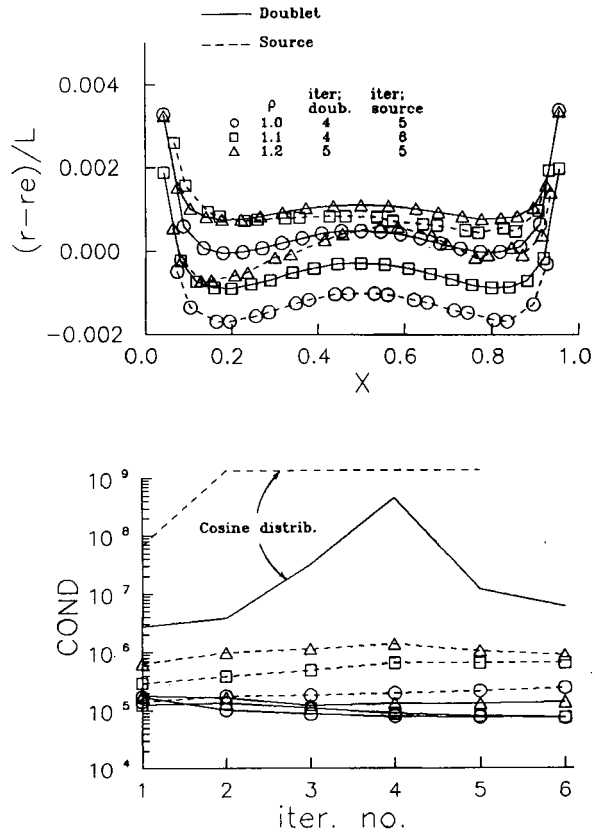

Figure 8. Effect of co-ordinate stretching in locating nodes on second-order inverse solutions for dumb-bell profile: (a) error in computed radius; (b) matrix condition number estimate

for this distribution are not shown in Figure 8(a) because of being substantially larger than those presented. In general we notice that the condition number increases with increasing degree of stretching for both methods. This is probably due to the control points near body ends becoming closer to each other, which increases the dependence among the matrix rows corresponding to these control points.

4.2.4. Effect of number of elements. This investigation is also limited to second-order methods. Two ellipsoids are used as test cases; one is thin with $f_r = 5$, while the other is thick with $f_r = 2$. The number of singularity elements, n_e, is varied between eight and 14 equal-length elements in steps of two. X_n and X_t are fixed at 0·02 and 0·98 for $f_r = 5$ and at 0·04 and 0·96 for $f_r = 2$ respectively. The distribution of the error in the computed radius along the body is given in Figure 9, while other results are summarized in Table III. For both ellipsoids we observe that the doublet method consistently gives lower error than the source method and that the matrix condition number for both methods increases with the number of elements. For $f_r = 5$ the error of both methods drops as n_e increases, while for $f_r = 2$ it decreases as n_e increases from eight to ten and then increases again with further increase in n_e. In fact, with 14 elements the doublet

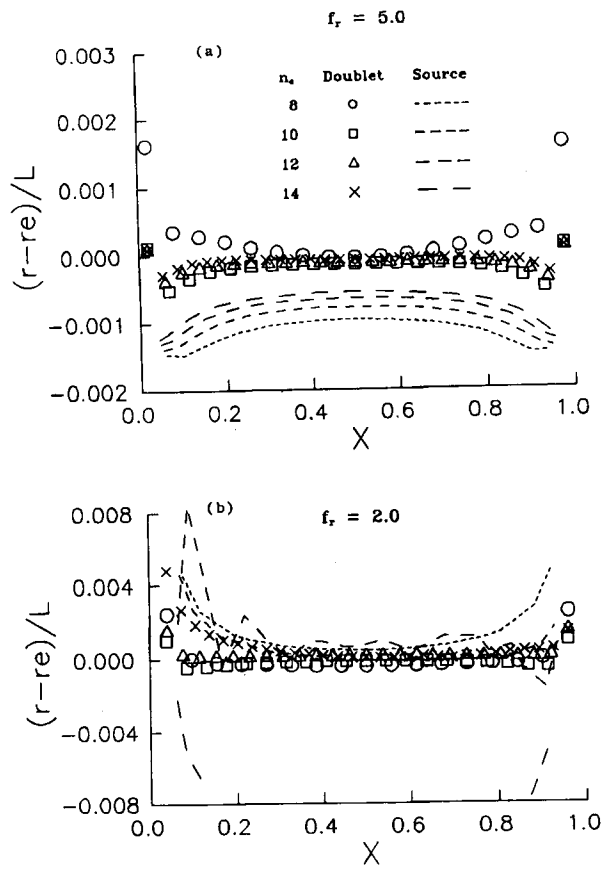

Figure 9. Effect of number of elements on error in radius as computed by second-order inverse methods for ellipsoids of revolution: (a) $f_r = 5$; (b) $f_r = 2$

Table III. Effect of number of elements on rate of convergence, matrix condition number and RMS error in computed radius for ellipsoids of revolution

	Second-order doublet method			Second-order source method		
n_e	Iter. no.	COND	ERMS	Iter. no.	COND	ERMS
			$f_r = 5{\cdot}0$			
8	3	$0{\cdot}702 \times 10^{5}$	$0{\cdot}330 \times 10^{-3}$	6	$0{\cdot}248 \times 10^{5}$	$0{\cdot}117 \times 10^{-2}$
10	4	$0{\cdot}134 \times 10^{6}$	$0{\cdot}236 \times 10^{-3}$	6	$0{\cdot}912 \times 10^{5}$	$0{\cdot}100 \times 10^{-2}$
12	4	$0{\cdot}223 \times 10^{6}$	$0{\cdot}159 \times 10^{-3}$	6	$0{\cdot}690 \times 10^{6}$	$0{\cdot}870 \times 10^{-3}$
14	4	$0{\cdot}352 \times 10^{6}$	$0{\cdot}117 \times 10^{-3}$	6	$0{\cdot}353 \times 10^{7}$	$0{\cdot}783 \times 10^{-3}$
			$f_r = 2{\cdot}0$			
8	5	$0{\cdot}638 \times 10^{7}$	$0{\cdot}509 \times 10^{-3}$	5	$0{\cdot}306 \times 10^{8}$	$0{\cdot}202 \times 10^{-2}$
10	6	$0{\cdot}323 \times 10^{9}$	$0{\cdot}293 \times 10^{-3}$	5	$0{\cdot}700 \times 10^{9}$	$0{\cdot}131 \times 10^{-2}$
12	6	$0{\cdot}488 \times 10^{9}$	$0{\cdot}297 \times 10^{-3}$	6	$0{\cdot}479 \times 10^{9}$	$0{\cdot}208 \times 10^{-2}$
14	5*	$0{\cdot}167 \times 10^{11}$	$0{\cdot}878 \times 10^{-3}$	3*	$0{\cdot}150 \times 10^{11}$	$0{\cdot}107 \times 10^{-1}$

* Solution diverged after this iteration.

method diverges for this thick body after the fifth iteration, in which a body with reasonably good accuracy is computed, while the source method diverges after the third iteration, where the computed body is quite far from the exact one. This different behaviour of error with n_e for the two bodies is attributed to the difference in matrix condition number. For $f_r = 5$ the matrix is well conditioned for all values of n_e and therefore higher n_e means better representation of the body and thus greater accuracy. For $f_r = 2$, although higher n_e is supposed to give better representation of the body, the sharp rise in COND with n_e (the matrix is near-singular for $n_e \geqslant 10$ for the doublet method and for $n_e \geqslant 8$ for the source method) causes the observed rise in error for $n_e \geqslant 12$. We further observe that the doublet method converges faster than the source method for $f_r = 5$ and at comparable rate for $f_r = 2$. The superior performance of the doublet methods is in spite of the fact that using ellipsoids as test cases favours source methods.[17]

Normalizing the co-ordinates by element length instead of body length reduced the matrix condition number sharply, sometimes by more than two orders of magnitude. This caused essentially no change in the computed radius in the cases where the matrix was originally not near-singular. In the cases with originally near-singular matrix the reduction in COND was not as dramatic and the effect on the results was not consistent.

5. CONCLUDING REMARKS

Higher-order line doublets have been used in an iterative scheme developed previously to solve the axisymmetric inverse problem in incompressible potential flow. The method has been verified in detail via carefully chosen test cases. The effect of the order of the distribution on the performance of the method was investigated and compared with that of the line source method. The performance was measured in terms of the accuracy of the computed radius, the speed of convergence and the coefficient matrix condition number. The sensitivity of the results to solution parameters such as insets and the number and distribution of elements along the axis was investigated.

Doublet methods were found to be generally more accurate and less sensitive to insets than source methods of the same order, especially for bodies with low f_r. Moreover, these methods had better-conditioned coefficient matrices and converged faster for bodies with moderate-to-high f_r. A second-order doublet method with equally spaced nodes or a slightly stretched node distribution appears to have the best performance. Increasing the number of elements provides better representation of the body; however, it increases the matrix condition number. Therefore we recommend the use of the maximum number of elements provided that the matrix does not become singular to computing accuracy. Ten second-order elements appear to be satisfactory for most bodies. The matrix condition number was also found to increase with the degree of stretching of the node distribution, the size of insets and sharply with the body thickness ratio for both methods. Increasing the insets above $0{\cdot}02L$ and up to $0{\cdot}06L$ from rounded ends slowed the convergence of both methods; however, it improved the accuracy of the doublet method and reduced the accuracy of the source method in general.

APPENDIX I: NOMENCLATURE

c_m	array for polynomial coefficients of singularity distribution over elements
COND	condition number estimate of coefficient matrix
ERMS	root mean square of error in computed radius r/L
f_r	body fineness ratio (length/maximum diameter)
L, l	body length and length of axial singularity element respectively
N	number of unknown polynomial coefficients of singularity distribution
n_c, n_e	number of control points and number of singularity elements respectively
n_{eq}	number of equations
q	local velocity on body surface
r	radial co-ordinate and local body radius
r_e	exact body radius
u, v	axial and radial components of q
V_∞	freestream velocity
x	axial co-ordinate starting at nose; $X = x/L$
x_n, x_t	axial location of beginning and end of singularity distribution respectively; $X_n = x_n/L$, $X_t = x_t/L$
ψ	Stokes stream function
μ, σ	intensities of doublet and source distributions respectively
ν	order of polynomial distribution over an element
ρ	parameter for stretching node distribution

APPENDIX II: CLOSED-FORM EXPRESSIONS OF INTEGRAL FUNCTIONS

The integral functions

$$H_k(\xi, \eta) = \int_0^l \frac{\zeta^k \, d\zeta}{[(\xi - \zeta)^2 + \eta^2]^{3/2}} \quad \text{and} \quad P_k(\xi, \eta) = \int_0^l \frac{\zeta^k \, d\zeta}{[(\xi - \zeta)^2 + \eta^2]^{5/2}}$$

are evaluated in closed form with the help of the CRC integration tables.[18] Defining the parameters $R_l = (\xi - l)^2 + \eta^2$ and $R_0 = \xi^2 + \eta^2$, after some algebraic manipulations we obtain

$$H_0 = \frac{1}{\eta^2}\left(\frac{\xi}{\sqrt{R_0}} - \frac{\xi - l}{\sqrt{R_l}}\right),$$

$$H_1 = \frac{1}{\eta^2}\left(\sqrt{R_0} + \frac{\xi l - R_0}{\sqrt{R_l}}\right),$$

$$H_2 = \frac{1}{\eta^2}\left(\xi\sqrt{R_0} - \frac{\xi^2(\xi - l) + \eta^2(\xi + l)}{\sqrt{R_l}}\right) + \ln\left(\frac{\sqrt{R_l} - (\xi - l)}{\sqrt{R_0} - \xi}\right),$$

$$H_k = \frac{l^{k-1}}{(k-2)\sqrt{R_l}} + \frac{2k-3}{k-2}\xi H_{k-1} - \frac{k-1}{k-2} R_0 H_{k-2} \quad \text{for } k \geqslant 3,$$

$$P_0 = \frac{1}{3\eta^2}\left(\frac{\xi}{R_0^{3/2}} - \frac{\xi - l}{R_l^{3/2}} + 2H_0\right),$$

$$P_1 = \frac{1}{3}\left(\frac{1}{R_0^{3/2}} - \frac{1}{R_l^{3/2}}\right) + \xi P_0,$$

$$P_2 = \frac{1}{3\eta^2}\left(\frac{\xi}{\sqrt{R_0}} - \frac{\xi^2(\xi - l) + \eta^2(\xi + l)}{R_l^{3/2}} + (2\xi^2 + \eta^2)H_0\right),$$

$$P_4 = -\frac{l^3}{2R_l^{3/2}} + \xi P_3 + H_2,$$

$$P_k = \frac{l^{k-1}}{(k-4)R_l^{3/2}} + \frac{2k-5}{k-4}\xi P_{k-1} - \frac{k-1}{k-4} R_0 P_{k-2} \quad \text{for } k = 3, k \geqslant 5.$$

REFERENCES

1. J. L. Kennedy and D. J. Marsden, 'The development of high lift, single-component airfoil sections', *Aeronaut. Q.*, **30**, 343–359 (1979).
2. K. R. Sirlatha, G. S. Dwarakanah and P. Ramamoorthy, 'Design of a natural laminar flow airfoil for a light aircraft', *J. Aircraft*, **27**, 966–968 (1990).
3. S. S. Dodbele, C. P. Van Dam, P. M. Vijgen and B. J. Holmes, 'Shaping of airplane fuselages for minimum drag', *J. Aircraft*, **24**, 298–304 (1987).
4. D. R. Bristow, 'A solution to the inverse problem for incompressible axisymmetric potential flow', *AIAA Paper No. 74–520*, 1974.
5. S. P. Dinavahi and S.-K. Chow, 'Inverse problem in incompressible irrotational axisymmetric flow', *J. Comput. Phys.*, **94**, 419–436 (1991).
6. M. F. Zedan and C. Dalton, 'Incompressible irrotational axisymmetric flow about a body of revolution: the inverse problem', *J. Hydronaut.*, **12**, 41–47 (1978); *AIAA Paper 77–1175*, 1977.
7. M. F. Zedan, A. Seif and S. Al-Moufadi, 'Drag reduction of airplane fuselages through shaping by the inverse method', *J. Aircraft*, **31**(1), (1994), in press.
8. M. F. Zedan and C. Dalton, 'Potential flow around axisymmetric bodies: direct and inverse problems', *AIAA J.*, **16**, 242–250 (1978).
9. M. F. Zedan and C. Dalton, 'Higher-order axial singularity distributions for potential flow about bodies of revolution', *Comput. Methods Appl. Mech. Eng.*, **21**, 295–314 (1980).
10. D. J. Jones, 'On the representation of axisymmetric bodies at zero angles of attack by sources along the axis', *Can. Aeronaut. Space J.*, **27**, 135–143 (1981).
11. G. S. Campell, 'Calculation of potential flow past simple bodies using axial sources and a least squares method', *J. Aircraft*, **21**, 437–438 (1984).
12. M. J. Hemsch, 'Improved, robust, axial line singularity method for bodies of revolution', *J. Aircraft*, **27**, 551–557 (1990).
13. J. M. Kuhlman and J.-Y. Shu, 'Potential flow past axisymmetric bodies at angle of attack', *J. Aircraft*, **21**, 218–220 (1984).
14. M. F. Zedan, 'Tuning the axial singularity method for accurate calculation of potential flow around axisymmetric bodies', *R. Aeronaut. J.*, submitted.

15. H. R. Vallantine, *Applied Hydrodynamics*, Butterworths, London, 1967.
16. G. E. Forsythe, M. A. Malcolm and C. B. Moler, *Computer Methods for Mathematical Computations*, Prentice-Hall, Englewood Cliffs, NJ, 1977.
17. J. Hess, 'The unsuitability of ellipsoids as test cases for line-source methods', *J. Aircraft*, **22**, 346–347 (1985).
18. S. M. Selby (ed.), *CRC Standard Mathematical Tables*, 15th edn, Chemical Rubber Co., Cleveland, OH, 1967.